The origin of large-scale magnetic flux dropouts

T. H. Zurbuchen, S. Hefti, L. A. Fisk, G. Gloeckler, and N. A. Schwadron
Department of Atmospheric, Oceanic and Space Sciences, University of Michigan, Ann Arbor

C. W. Smith, N. F. Ness
Bartol Research Institute, University of Delaware, Newark

R. M. Skoug, D. J. McComas
Los Alamos National Laboratory, Los Alamos

L. F. Burlaga
Goddard Space Flight Center, Greenbelt

Short title: MAGNETIC FLUX DROP-OUTS

Abstract. Magnetic holes are sudden changes in the magnetic field intensity |**B**| from typical interplanetary values (about 10 nT) to less than 1 nT in a matter of seconds. The intensity then recovers seconds up to 30 minutes later. These |B| dropouts can be seen daily; less often observed, but even more dramatic, are magnetic field depletions that last for up to 1 hour. We use selected periods of magnetic flux drop-outs observed with various sensors of the Advanced Composition Explorer (ACE) with a unique combination of magnetic field, plasma and composition experiments to establish the origin of these peculiar objects. Based on this combination of plasma, field and composition data we conclude that these magnetic flux drop-outs very likely are born in the heliosphere and are not of direct solar origin. We also suggest a possible formation mechanism which is associated with magnetic reconnection close to the Sun.

1. Introduction

The occurrence of short-term magnetic flux drop-outs, so-called magnetic holes (MH), within the solar wind was first described by *Turner et al.* in [1977] using IMP 6 data. They described isolated, pressure-balanced structures with variable widths for which the magnetic field intensity $|\mathbf{B}|$ dropped to less than 1 nT. They were described to occur at a rate of approximately 1.5 holes per day. The width of the holes ranged from 2 to 130 sec with a median of 50 sec, corresponding to a scale of around 200 proton gyro radii. In approximately 30% of these cases, the magnetic field did not change direction within 5°. In other cases the magnetic field direction was observed to change rather abruptly, sometimes erratically varying throughout the |B|-depletion period. A more extended study was recently performed by *Winterhalter et al.* [1994, 1995] who analyzed the Ulysses data-set from 1990 to the end of 1992. During this time Ulysses moved between 1 AU to 5.4 AU, from the ecliptic to a Southern latitude of 23°. Magnetic holes were found over the full ranges of heliocentric distance and latitudes. The typical width was observed to be in the range of 5-50 sec with a most probable value of 22 sec. This compares very well with the *Turner et al.* [1977] data. One important selection criteria may be reflected in the fact that the longest magnetic hole observed lasted 150 sec. Even more recently *Sperveslage et al.* [2000] used a combination of Voyager and Helios data to perform a comprehensive statistical analysis on magnetic depletion events. Even though their occurrence rate seems to be slightly declining with increasing heliocentric distance, MH are observed from 0.3 AU to 17 AU. It is worth mentioning that there is a bias against more extended MH in both, the *Winterhalter et al.* [1994] and the *Sperveslage et al.* [2000] analysis. They both use a sliding window with a length of 300 s to detect MH, even though magnetic field depletions are observed to much longer scales. Figure 1 shows three examples of magnetic holes on a temporal scales from several seconds to 1 hour. These longer |B|-depletions occur less often, but carry all the defining properties of "magnetic holes". They are not associated with large-scale polarity changes of the background magnetic field and do not have any direct association with Coronal Mass Ejections (CMEs).

Figure 1

Geometrically extended magnetic field depletions were first described by *Burlaga* [1968]. This analysis was based on plasma and magnetic field data. It was argued that these larger scale magnetic field depletions were a signature of reconnection in the solar wind, resulting in directional discontinuities ("D-sheets"). It was also pointed out that these discontinuities are most likely tangential in nature [*Burlaga and Ness*, 1968; see, also for MH *Chisham et al.*, 2000]. The process responsible for the formation of D-sheets can be illustrated using two adjacent fluxtubes of anti-parallel field. These fluxtubes are initially separated by a tangential discontinuity. If at this interface region the conductivity

and viscosity are finite, then annihilation of neighboring field-lines will reduce the magnetic field intensity and locally increase the plasma density and/or temperature. A simple model introduced by *Burlaga* [1968] relates the minimum magnetic field intensity and the magnetic field vectors which are not affected by this reconnection process. These D-sheets were also investigated with plasma data, but no identifying signature (such as increase density and temperature) was found.

The three-dimensional structure of MH is not well known. For some relatively rare cases multi-spacecraft observations are available. For example, *Fitzenreiter and Burlaga* [1978] analyzed short magnetic holes using IMP5 and IMP 6 data. These combined data showed that, at least for four specific cases, the current sheets are approximately planar. This motivated a series of one-dimensional models [see, e.g., *Burlaga and Lemaire,* 1978; *Baumgärtel,* 1999]. Most of these models consider short magnetic depletions which occur on a spatial scale comparable to several ion gyro-radii. *Burlaga and Lemaire* [1978] used a static kinetic model, solving Vlasov's equation for this geometry. *Winterhalter et al.* [1994] showed evidence for the association of small-scale magnetic holes with the mirror-mode instability. Most recently, *Baumgärtel* [1999] used a soliton description for these structures.

However, the more extended holes of interest in this study last up to hours and are therefore not on a kinetic scale. The models proposed for D-sheets fall into two categories, reconnection based models, and pressure-balance models. Note that these two descriptions do not have to be mutually exclusive. Convected structures in the solar wind tend to evolve towards pressure-balance, rather independently of their respective origins.

This study concentrates on extended MH with a large geometrical scale, extending at least 0.5 hours at ACE.

1. Are extended magnetic depletions of solar origin, or do they occur in interplanetary space ?

2. What are the physical processes relevant for the appearance of these MH ?

We will address these questions using a complete set of composition, plasma, and magnetic field data from ACE. After introducing the data-sets in section 2, we will present a summary of plasma and composition signatures of MH. In section 4 we will present a simple model for these extended MH which is consistent with these data.

2. Data Descriptions

For this study we use data from ACE which is equipped with a complete plasma and composition package. It has provided near-full time coverage with state-of-the-art solar wind data since shortly after its launch in August 1997 [*Stone et al.*, 1998]. For this particular study we use a combined set of plasma,

magnetic field and composition data. We use 15 sec averages of the magnetic field vectors measured by the Magnetic Field Experiment (MAG) [*Smith et al.*, 1998]. The bulk plasma properties, as well as the electron distribution functions are measured by the Solar Wind Electron Proton and Alpha Monitor (SWEPAM) [*McComas et al.*, 1998]. Proton data have 64 sec time-resolution, electron data have 128 sec resolution. Solar wind composition data are provided by the Solar Wind Ion Composition Spectrometer (SWICS) [*Gloeckler et al.,* 1998] with a time resolution of 12 min. Figures 2a-g and Figures 3a-d show an example of an extended magnetic hole including data from these three instruments which will now be discussed in detail. This event is equivalent to the event shown in the top-panel of Figure 1 and happened on March 10, 1998 between 11:45–12:45 UT. Figures 2 show the defining plasma and field data, Figures 3 show composition data, and pitch-angle distributions of supra-thermal electrons.

Figures 2

Figures 3

2.1. Magnetic Field and Plasma Data

Figure 2 shows the characteristic decrease of the magnetic flux during a period of almost one hour. The time axis has been chosen to be centered close to the minimum values of the magnetic flux. The magnetic pressure depletion is generally well balanced by the kinetic pressure. In this example, the enhancement of the kinetic temperature of electrons and protons is the most significant contribution to this increased kinetic pressure.

This is illustrated in Figure 2b-e showing solar wind speed v, proton density n, proton temperature $T_{\rm p}$, and electron temperature $T_{\rm e}$ as measured by SWEPAM. Within the magnetic depletion area, $T_{\rm p}$ increases by around a factor of 5, $T_{\rm e}$ by a smaller factor. The density n does not show any particular signature limited to the magnetic depletion, and v shows a small, but significant increase.

Figure 2f-g (together with Figure 2a) show the magnetic field vector B in spherical heliospheric coordinates (B, θ, ϕ). The angle θ measures the latitude with respect to the solar equatorial plane, i.e., for a nominal Parker spiral $\theta = 0°$. The winding angle ϕ is defined in the same plane relative to the radially outward direction. For a Parker angle of 45°, $\phi = -45° = 315°$ for outwards field polarity and $\phi = 135°$ for inwards polarity. Special attention has been given to the time-periods when $B \approx 0$ nT. The magnetic field vector shows a distinct rotation within the magnetic field depletion. It starts in an approximate Parker orientation and rotates substantially, reaching the opposite polarity within the magnetic depletion. Also θ shows significant excursions, exceeding 80° during the time of maximal excursion of ϕ.

2.2. Composition Signatures

Figures 3c-d show $n_{O^{+7}}/n_{O^{+6}}$ as well as the elemental ratio of n_{Fe}/n_O for the entire solar time-interval of question. As previously pointed out, the maximum time-resolution for these quantities is determined by the instrument cycle of 12 min. This turns out to be crucial for the current analysis. The elemental abundance n_{Fe}/n_O is observed to be very variable in the solar wind, much more variable than high-speed, coronal hole associated wind. It has been suggested [see e.g. *Zurbuchen et al.* 1998] that this is naturally interpreted as a fingerprint of fractionation processes in closed magnetic structures, such as coronal loops. This has more recently been confirmed based on time-dependent remote observations by Solar and Heliospheric Observatory (SOHO) [*Feldman et al.* 1998]: when large coronal loops emerge from the photosphere, they appear to have essentially photospheric composition. The plasma associated with these loops is then observed to undergo fractionation on a time-scale of $\sim 10^5$ s. This fractionation increases the relative abundance ratio of elements of low first ionization potential (FIP) relative to high-FIP elements. The FIP-fractionation factor of each individual magnetic loop varies quite substantially, perhaps due to processes such as described by *Schwadron et al.* [1999]. If these loops are the source of the low-speed solar wind, as first suggested by *Axford et al.* 1977, the large variations of n_{Fe}/n_O are naturally explained. The release process of this plasma is presumably associated with reconnection. It has been pointed out that such reconnection processes are necessary, and implied by basic physical processes such as differential rotation and the equilibration of magnetic pressures in the low corona [*Fisk et al.* 1999]. Compositional variations are therefore compositional fingerprints of source regions of respective solar wind streams.

The physical meaning of the charge state ratio $n_{O^{+7}}/n_{O^{+6}}$ has been addressed previously [*Bürgi and Geiss,* 1986; *Hefti et al.,* 2000]. Due to its quick freeze-in process, $n_{O^{+7}}/n_{O^{+6}}$ turns out to be another very useful tracer for the solar wind source regions. A cold source, such as a coronal hole, will cause low $n_{O^{+7}}/n_{O^{+6}} \simeq 0.1$; hot sources, such as solar wind associated with streamers, have a clearly higher $n_{O^{+7}}/n_{O^{+6}} \simeq 0.7$. In the case of low-speed solar wind a large amount of scattering is observed, which has been interpreted to be associated with an inhomogeneous, time-variable solar wind source [*Zurbuchen et al.* 2000]. It is important to note that two plasma parcels starting at exactly the same temperature may exhibit different $n_{O^{+7}}/n_{O^{+6}}$ if their density-profiles and/or speed-profiles are distinctly different between the solar wind source and the freeze-in point below 1 solar radius (R_s) from the photosphere.

The n_{Fe}/n_O ratio would be expected to be different if these magnetic field depletions are associated with a different, peculiar source region in the photosphere. If these depletions were of solar origin,

compositional signatures would be even more distinct for $n_{O^{+7}}/n_{O^{+6}}$, because this quantity carries additional signatures due to the difference in expansion profile suggested by the 1 AU situation. This is clearly not the case, as shown in Figure 3a+b. Within statistical limits, the $n_{O^{+7}}/n_{O^{+6}}$ and n_{Fe}/n_O ratios in the MH are the same as the composition outside. Note, that the MH is observed to be embedded into a composition variation on a scale much larger than the scale of the magnetic depletion, with a transition right through the MH. Both compositional signatures therefore do not support a solar origin of this magnetic flux drop-out.

2.3. Electron Pitch Angle Distributions

Figure 3a shows electron pitch angle distributions (EPAD) for the energy of 272 eV. Pitch angle distributions of electrons in this energy range are a sensitive tracer for the magnetic field topology. *Feldman et al.* [1999] discuss electron pitch angle distribution functions which are similar to the ones shown in Figure 3c.

It is obvious from Figure 3a that there is a clear dependence of the observed EPAD throughout the magnetic depletion event: outside of the MH the pitch-angle distribution is peaked along the magnetic field and becomes increasingly isotropic towards the center of the magnetic flux drop-out. Roughly, the level of anisotropy correlates with the magnetic field strength. Figure 3b shows the relative level of fluctuations on the shortest time-scales accessible to MAG, with means and variances computed on 16 sec intervals. The relative level of fluctuations $(\delta B/B)^2$ is observed to be rather intermittent, but clearly enhanced during time-periods of reduced magnetic field magnitude. We will now discuss that this enhancement is very crucial for the understanding the observed EPAD.

In the absence of scattering one would expect adiabatic focusing to strongly increase the anisotropy, as opposed to the observed decrease, since, for a single particle,

$$\frac{dv_\parallel}{dz} = -\frac{v_\perp^2}{B}\frac{\partial B}{\partial z}. \tag{1}$$

Due to the dramatic depletion of the magnetic field from typical interplanetary values, one would therefore expect a strongly beamed, highly anisotropic EPAD. However, this effect is compensated by the increased scattering. This can be shown using the following order of magnitude estimate.

Scattering balances the enhanced focusing, if

$$\frac{v_\perp^2}{\lambda} \sim \frac{v_\parallel}{\tau} \tag{2}$$

The first term is an order of magnitude estimate of Equation 1 assuming that the geometrical scale of the MH is λ. The scattering time τ is related to the mean-free-path as follows $\tau = \lambda_{\rm mfp}/v$. If the

distribution is close to isotropy, $v_\perp \sim v_\parallel$. From this order of magnitude estimate we therefore conclude that the focusing can be compensated for by scattering if

$$\lambda_{\rm mfp}/\lambda \leq 1. \tag{3}$$

Using the scaling $\lambda_{\rm mfp} \propto (\delta B/B)^{-2}$ and since the scattering mean-free-path in the unperturbed solar wind is ~ 1 AU, $\lambda_{\rm mfp}$ can be estimated from Figure 3b. The condition given in Equation 3 is found to be easily fulfilled for all reasonable λ values. It is therefore not unreasonable to interpret the observed almost-isotropic EPAD to be a result of increased scattering due to an enhanced $(\delta B/B)^2$ when the magnetic flux is reduced.

Finally, note that complete isotropy is also achieved during solar wind Heat-Flux Dropouts (HFD). These HFD occur when magnetic field-lines are disconnected from the Sun [see, e.g., *Larson et al.*, 1997]. It is unlikely that magnetic holes are associated with such events. Here, the total flux of the supra-thermal electrons remains approximately constant during the entire event. Also, in many cases, there is a very small anisotropy which can be found in the data throughout the magnetic depletion period.

3. Statistical Study

We have performed a statistical study of extended magnetic field depletions occurring between the beginning of February and the end of July of 1998. During this time-period there are 12 extended MH. All these extended holes are identified based on the magnetic field depletion. Also, it was carefully checked that these depletions were not associated with CMEs and the heliospheric current sheet. During two of the events SWICS was not in its nominal data access mode, the remaining 10 cases were included in this study. The exact times are given in Table 1. A second example is given in Figure 4 and Figure 5 using the same format as described above. This magnetic depletion period was observed April 3 from 4:00–5:30 UT. All basic features described in the previous section still apply. Most noticeably, there are no distinct compositional signatures associated with the magnetic field depletion. Also, the EPAD is much closer to isotropy within the magnetic hole than outside, or in the side-lobes of the structure. One minor exception concerns the rotation of the magnetic field which is reduced compared to the first case, but still shows significant rotations away from the average Parker field direction. Again, longitude, and latitude rotations are clearly seen. In this case, the density increase, shown in Figures 4c, is the most relevant contribution to the increased kinetic pressure.

Table 1

Figure 4

Figure 5

The longest magnetic flux depletion event is shown in Figures 6 and Figure 7 in the same format as Figures 2 and Figure 3. This event took place between April 17, 1998 from 5:45-10:00 UT, affecting

Figures 6

Figure 7

more than 4 hours worth of data. Similar to the second example, the density enhancement is primarily responsible for the establishment of pressure-balance. Here the rotations are rather erratic, as shown in Figure 6f-g. Note, particularly, a strong θ deflection out of the equatorial plane for almost the entire interval. Also, the small-scale structure of these rotations seems to be well correlated with the magnetic field magnitude variations. Figure 7shows unchanged composition for $n_{O^{+7}}/n_{O^{+6}}$ and n_{Fe}/n_O .

The results can be summarized as follows.

1. None of the 10 cases has n_{Fe}/n_O signatures: This strongly suggest a heliospheric origin of these magnetic depletions. The observed n_{Fe}/n_O ratio is consistent with low-speed solar wind.

2. None of the events has correlated $n_{O^{+7}}/n_{O^{+6}}$ signatures: This suggests a common solar wind expansion history for the plasma. The observed $n_{O^{+7}}/n_{O^{+6}}$ ratio is consistent with low-speed solar wind.

3. All events are approximately pressure-balanced. For most of the cases, the events (9 out of 10) are associated with a strong increase of the solar wind density. In some cases (4/10) there are also significant increases in kinetic temperature. This is in common with magnetic holes.

4. All events are associated with large to moderate ($> 90°$) magnetic field rotations, often up to 180°. This looks very similar to the previously mentioned "D-sheets".

5. All events are associated with a more isotropic electron distribution function within magnetic depletion regions. This is very likely due to enhanced magnetic turbulence $(\delta B/B)^2$ in these regions.

4. Model for Extended Magnetic Field Depletions

It is the purpose of this section to devise a model which addresses all constraints pointed out in the previous chapter. This model presented here should not be understood as a unique solution, but rather a successful candidate for extended magnetic field depletion events. The model is sketched in Figure 8.

We propose here that these MH are caused through magnetic reconnection in the high corona, beyond the critical point. For the initial conditions, as shown in Figure 8, a magnetic loop extends into the far corona. This closed structure can then reconnect with a open magnetic field line. This generally happens within the Alfvenic point, perhaps in a geometry which is sketched in Figure 8a. During this process, the density and temperature can locally increase due to several reasons. One method was mentioned in section 1 in connection with D-sheets: magnetic field annihilation at the reconnection point can have a direct effect on plasma temperature and density (for details, refer to *Burlaga* [1968]). There is also another effect which is sketched in Figure 8: the U-type structure resulting in this reconnection event accelerates away from the Sun under the influence of the tensional effect of the bent

magnetic field. In this process the accelerated structure will sweep up plasma, therefore increasing the kinetic pressure. Kinetic temperature enhancements may be expected due to heating effect of the reconnection, density and temperature enhancements are produced by the inertial effect of plasma in the accelerated system and the associated adiabatic compression. This process is limited by the build-up of a field-aligned kinetic pressure gradient preventing further accumulation.

This scenario is consistent with all results summarized above: One would not expect any compositional signatures (consistent with 1. and 2.) since the magnetic field is associated with standard slow solar wind. The density and temperature enhancements in this model are, as described, the cause for the magnetic field depletion (consistent with 3.) and therefore crucial for the validity of this idea. The magnetic field signatures are necessarily very close to the Sun, and cannot be lost once the solar wind flow goes super-Alfvenic (consistent with 4.). As previously pointed out, EPAD signatures can be understood as a signature of scattering in the heliosphere, and are not solar in origin (consistent with 5.). Note that the situation shown in Figure 8 is very typical for increased solar activity: the loop has a polarity opposite to the ambient magnetic field. Reconnection processes as discussed here could have a major effect on the large-scale restructuring of the heliospheric magnetic field transporting open magnetic flux of a given polarity to the opposite hemisphere.

This model bears much similarity to the D-sheet concept put forth by *Burlaga* [1968]. The magnetic intensity depletions look remarkably similar for both studies. However, we observe significant plasma signatures as opposed to the previous studies. A more detailed comparison with the D-sheet concept is beyond the scope of this study and will be the topic of a follow-up investigation.

5. Concluding Remarks

The extended magnetic depletion regions are a very interesting case-study which shows the power of combining modern plasma, composition and field measurements. A successful model has to address all constraints coming from these data at the same time.

The proposed model addresses all the experimental constraints with a reconnection effect which is presumably very common in the low corona. It is not clear to what extent this interpretation is also applicable for smaller MH. At very small scales kinetic effects are likely to play a role and our interpretation may not be applicable. This is particularly true for linear MH which do not exhibit any directional change of the magnetic field, which is crucial for our explanation. It is therefore suggested that the large-scale magnetic flux depletions are very different from small-scale MH as, for example, described by *Winterhalter et al.* [1994].

Acknowledgments. THZ acknowledges helpful discussions with P. Koehn. The University of Michigan part of this work was supported, in part, by NASA contracts NAG5-2810 and NAG5-7111. NAS and THZ were also supported, in part, by NASA grant NAG5-6471 and NSF grant ATM 9714070. Support of NFN and CWS was provided by subcontract PC251439 to the Bartol Research Institute under NASA grant NAG5-6912 for support of the ACE Magnetic Field Experiment.

References

Axford, W. I., The three-dimensional structure of the interplanetary medium, in the Study of Traveling Interplanetary Phenomena, ed M. A. Shea et al., Dortrecht, Reidel, 1977.

Baumgärtel, K., Soliton approach to magnetic holes, *J. Geophys. Res., 104*, 28,295, 1999.

Bürgi, A., and J. Geiss, Helium and minor ions in the corona and solar wind – Dynamics and charge states, *Sol. Phys., 103*, 347, 1986.

Burlaga, L. F., Micro-structures in the interplanetary medium, *Solar Phys., 4*, 67, 1968.

Burlaga, L. F., and N. F. Ness, Macro-and micro-structure in the interplanetary magnetic field, *Canad. J. of Phys., 46,* S962, 1968.

Burlaga, L. F., and J. F. Lemaire, Interplanetary magnetic holes: theory, *J. Geophys. Res., 83*, 5157, 1978.

Chisham, G., S. J. Schwartz, D. Burgess, S. D. Bale, M. W. Dunlop and C. T. Russell, Multisatellite observations of large magnetic depressions in the solar wind, *J. Geophys. Res.*, *105*, 2325–2335, 2000.

Feldman, U., FIP effect on the solar upper atmosphere: Spectroscopic results, *Space Sci. Rev., 85,* 227, 1998.

Feldman, W. C., R. M. Skoug, J. T. Gosling, D. J. McComas, R. L. Tokar, L. F. Burlaga, N. F. Ness, and C. W. Smith, Observations of suprathermal electron conics in an interplanetary coronal mass ejection, *Geophys. Res. Lett., 26*, 2613, 1999.

Fisk, L. A., T. H. Zurbuchen, and N. A. Schwadron, On the coronal magnetic field: Consequencs of large scale motion, *Astrophys. J., 521*, 868, 1999.

Fitzenreiter, R. J., and L. F. Burlaga, Structure of current sheets in magnetic holes at 1 AU, *J. Geophys. Res.*, *83*, 5579–5585, 1978.

Gloeckler, G., et al. Investigation of the composition of solar and interstellar matter using solar wind and pickup ion measurements with SWICS and SWIMS on the ACE spacecraft, *Space Sci. Rev.*, *86*, 495, 1998.

Hefti, S., H. Grunwaldt, P. Bochsler, and M. Aellig, Oxygen freeze-in temperatures measured with SOHO/CELIAS/ CTOF, *J. Geophys. Res.,* in press, 2000.

Larson, D. E., et al., Tracing the topology of the October 18-20, 1995 magnetic cloud with $\sim$ 0.1-120 keV electrons, *Geophys. Res. Lett.,* , *24*, 1911, 1994.

McComas, D. J., S. J. Bame, P. Barker, W. C. Feldman, J. L. Phillips, P. Riley, and J. W. Griffee, Solar wind electron proton alpha monitor (SWEPAM) for the advanced composition explorer, *Space Sci. Rev.*, *86*, 563, 1998.

Schwadron, N. A., L. A. Fisk, and T. H. Zurbuchen, Elemental fractionation in the slow solar wind, *Astrophys. J., 521,* 859, 1999.

Smith, C. W., J. L'Heureux, N. F. Ness, M. H. Acuna, L. F. Burlaga, and J. Scheifele, The ACE magnetic field experiment, *Space Sci. Rev.*, *86*, 613, 1998.

Stone, E. C., A. M. Frandsen, R. A. Mewaldt, E. R. Christian, D. Margolies, J. F. Ormes, and F. Snow, The Advanced Composition Explorer, *Space Sci. Rev., 86*, 1, 1998.

Turner, J. M., L. F. Burlaga, N. F. Ness, and J. F. Lemaire, Magnetic holes in the solar wind, *J. Geophys. Res., 82*, 1921, 1977.

Sperveslage, K., F. M. Nebauer, K. Baumgärtel, and N. F. Ness, Magnetic holes in the solar wind between 0.3 AU and 17 AU, *Nonlin. Proc. Geophys.,* in press, 2000.

von Steiger, R. et al., Composition of quasi-stationary solar wind flows from SWICS/Ulysses, submitted to *Journal of Geophysical Research*, 1999.

Winterhalter, D., M. Neugebauer, B. E. Goldstein, E. J. Smith, S. J. Bame, and A. Balogh, Ulysses field and plasma observations of magnetic holes in the solar wind and their relation to mirror-mode structures *J. Geophys. Res., 99*, 23,371, 1994.

Winterhalter, D., M. Neugebauer, B. E. Goldstein, E. J. Smith, B. T. Tsurutani, S. J. Bame, and A. Balogh, Magnetic holes in the solar wind and their relation to mirror-mode structures, *Space Science Reviews*, *72*, 201, 1995.

Zurbuchen, T. H., L. A. Fisk, G. Gloeckler, and N. A. Schwadron, Element and isotopic fractionation in closed magnetic structures, *Space Sci. Rev., 85*, 397, 1998.

Zurbuchen, T. H., S. Hefti, L.A. Fisk, G. Gloeckler, and N. A. Schwadron, Magnetic structure of the slow solar wind: Constraints from composition data, *J. Geophys. Res.,* in press, 2000.

L. A. Fisk, G. Gloeckler, S. Hefti, N. A. Schwadron, and T. H. Zurbuchen, Space Physics Research Laboratory, University of Michigan, 2455 Hayward Street, Ann Arbor, MI 48109-2143. (e-mail: lafisk@umich.edu; gg10@umail.umd.edu; hefti@pooh.engin.umich.edu; nathanas@umich.edu; thomasz@umich.edu)

C. W. Smith, and N. F. Ness, Bartol Research Institute, University of Delaware, Newark, DE 19716

R. M. Skoug, and D. J. McComas, Los Alamos National Laboratory, MS D466, Los Alamos, NM 87545

L. F. Burlaga, NASA Goddard Space Flight Center, MC 692, Greenbelt, MD 20771-0001

Received _____

To appear in the *Journal of Geophysical Research*, 2000.

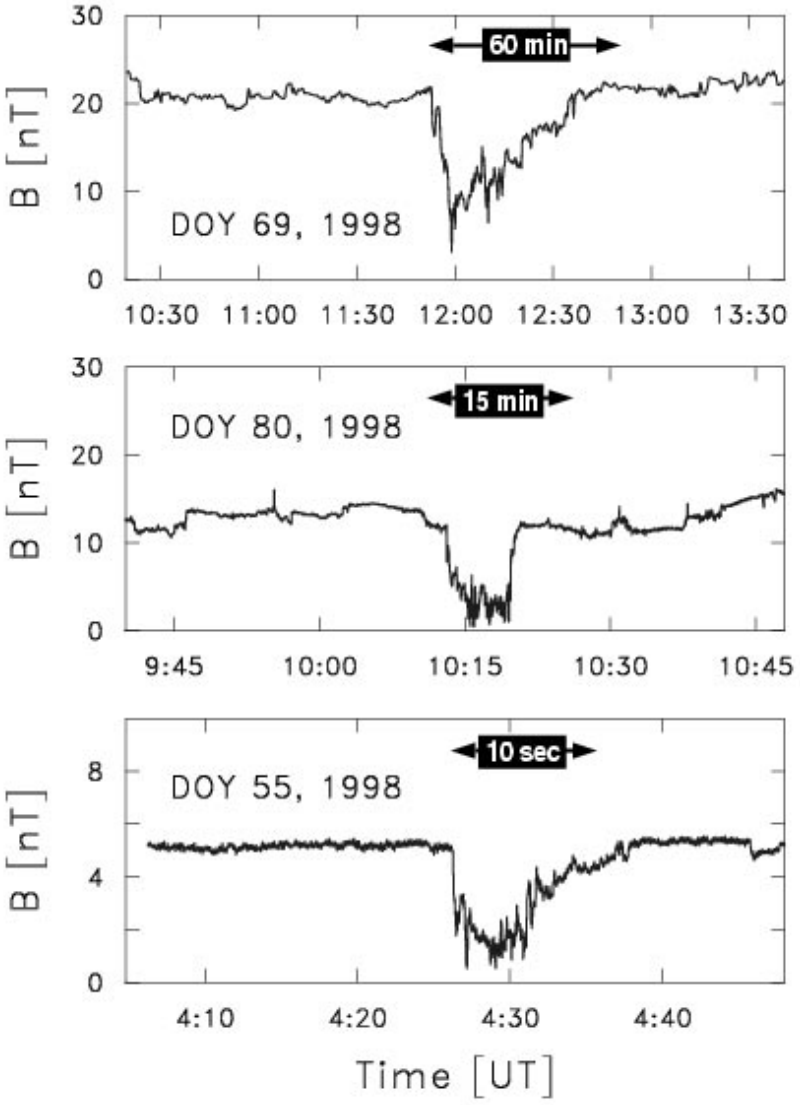

Figure 1. Magnetic depletions observed on ACE. These depletions occur on a variety of scales, from seconds to hours. In this study we concetrate on large-scale magnetic depletions such as shown in the first two panels.

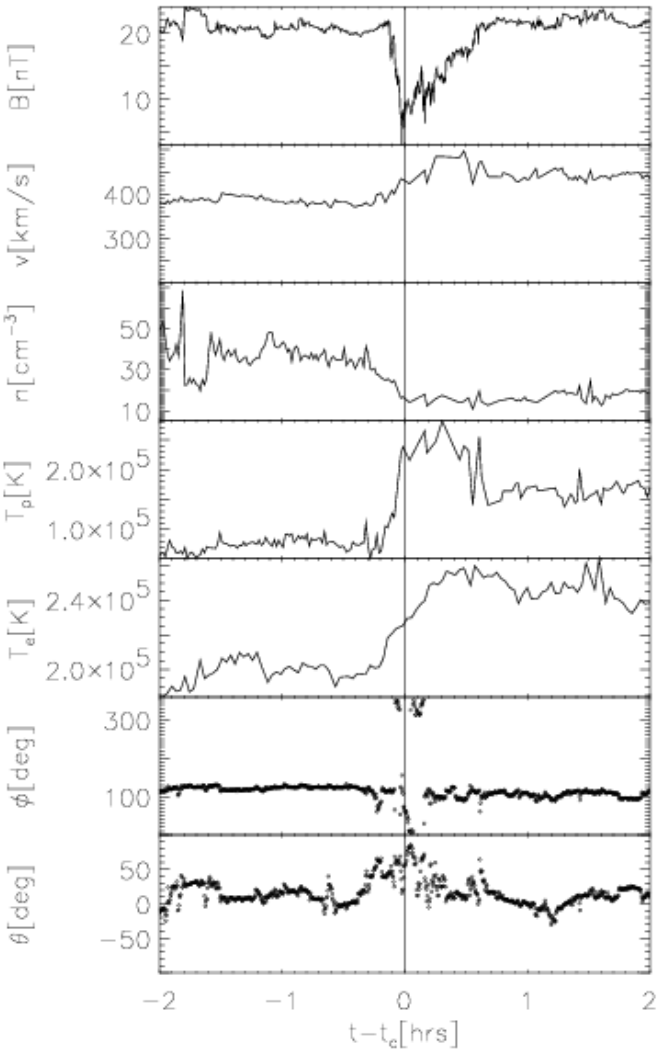

Figure 2. Plasma data from MAG, and SWEPAM for the magnetic depletion of March 10. The data is centered with repect to the minimum magnetic field. We show from top to bottom, magnetic field magnitude, proton speed, density and temperature, electron temperature, and the magnetic field latitude and longitude in RTN. For more details refer to text.

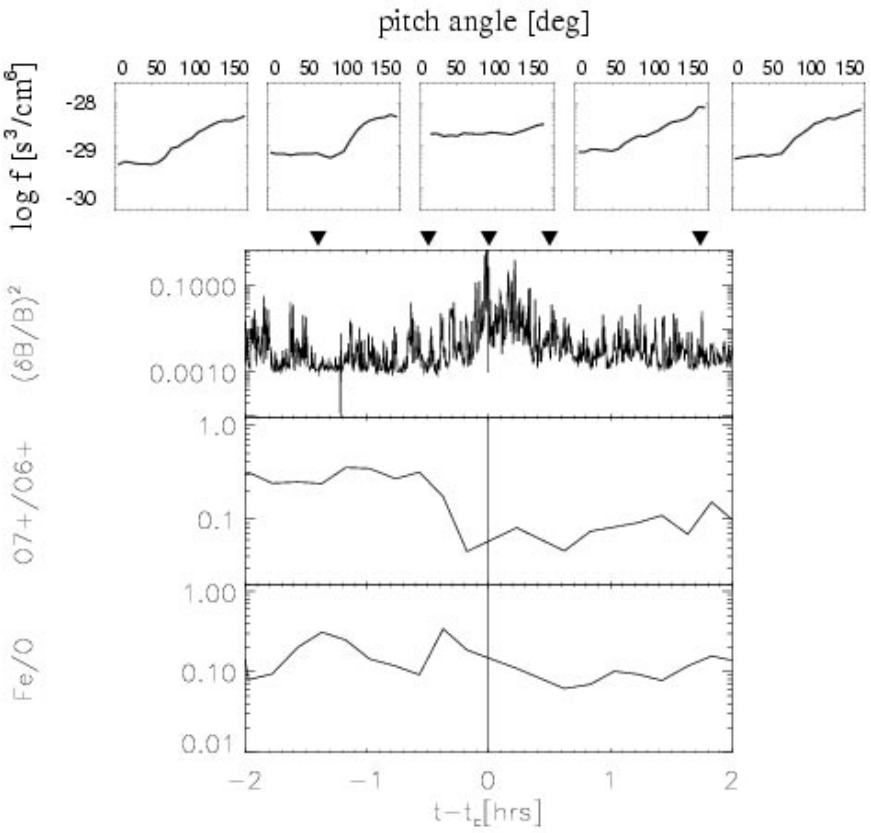

Figure 3. Electron pitch-angle and composition information for the same event as shown in Figure 2. We show from top to bottom electron pitch angle distribution for 272 eV electrons during five selected 2 minute intervals, the magnetic fluctuation level at high frequency, and $n_{O^{+7}}/n_{O^{+6}}$ and n_{Fe}/n_O . For details and discussion refer to text.

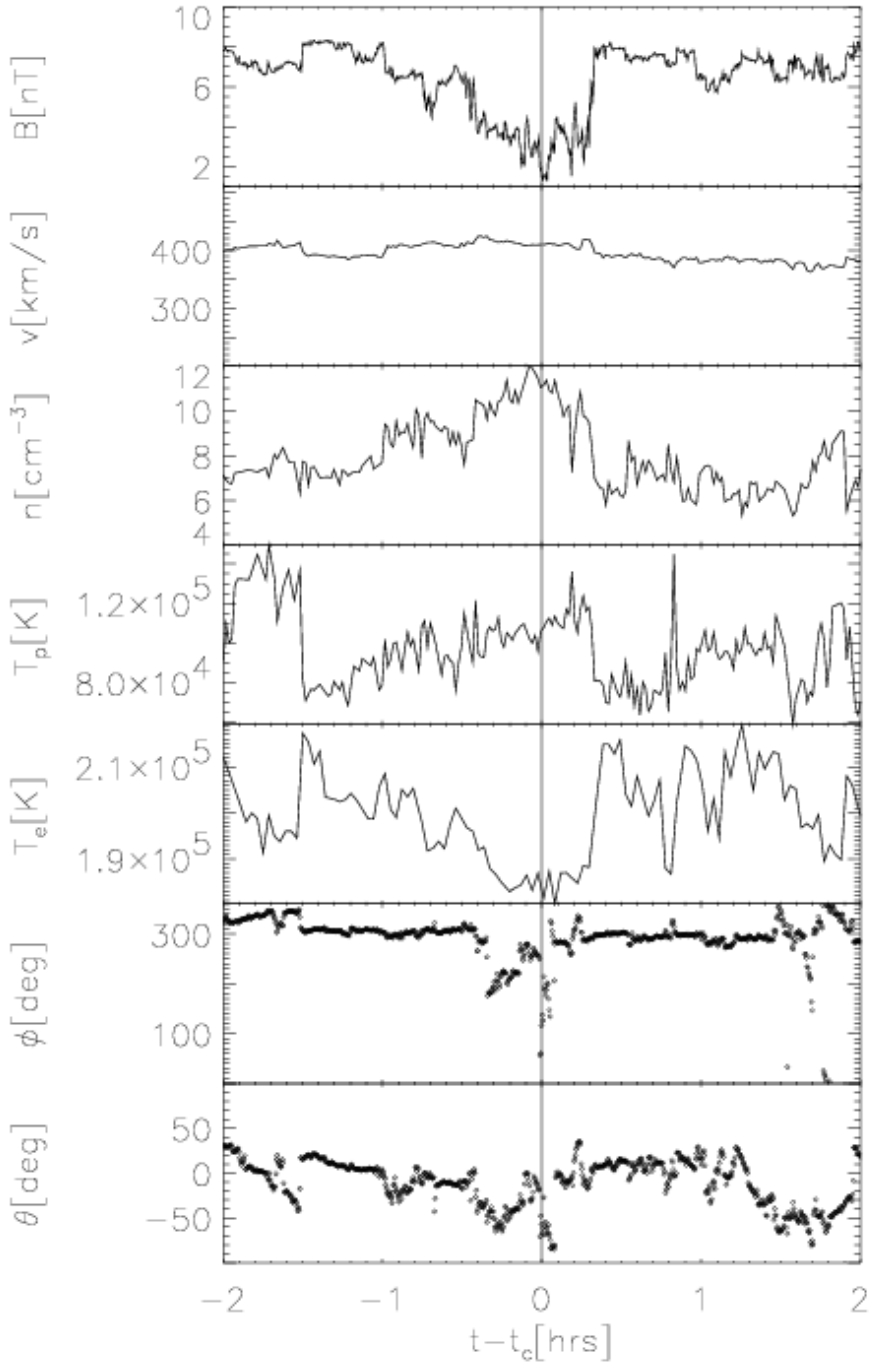

Figure 4. Plasma data from MAG and SWEPAM for the event during April 3. We use the same format as in Figure 2.

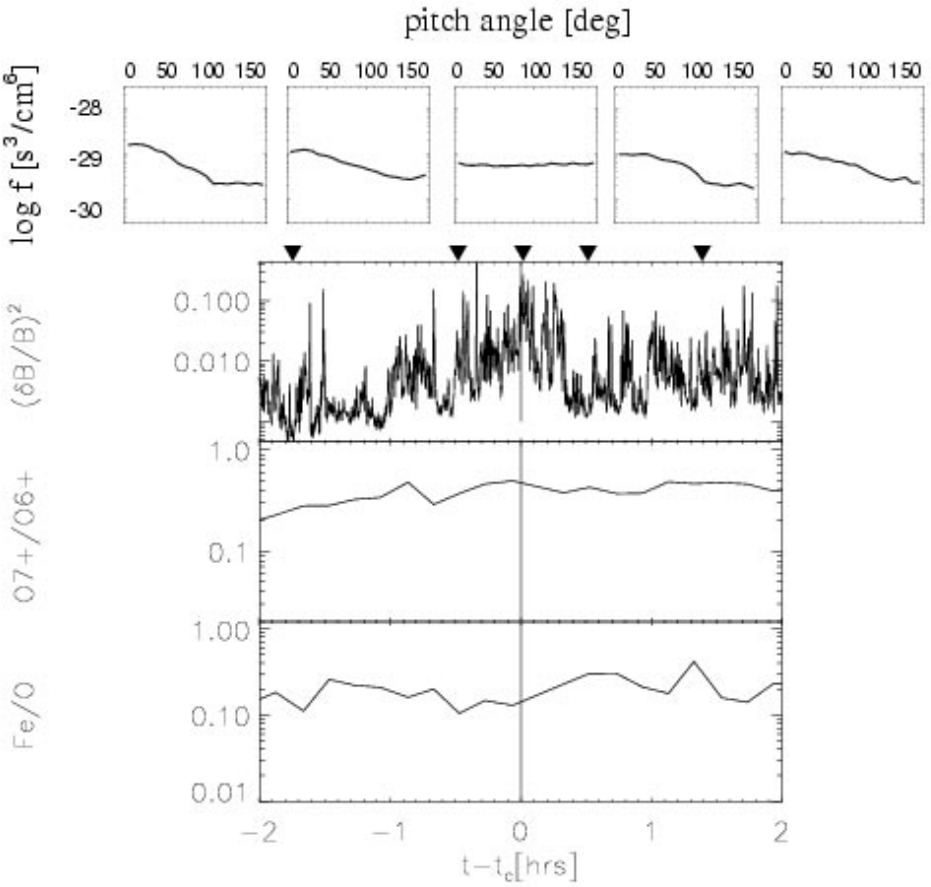

Figure 5. Electron pitch-angle and composition information for the event shown in Figure 4. The format is the same as in Figure 3.

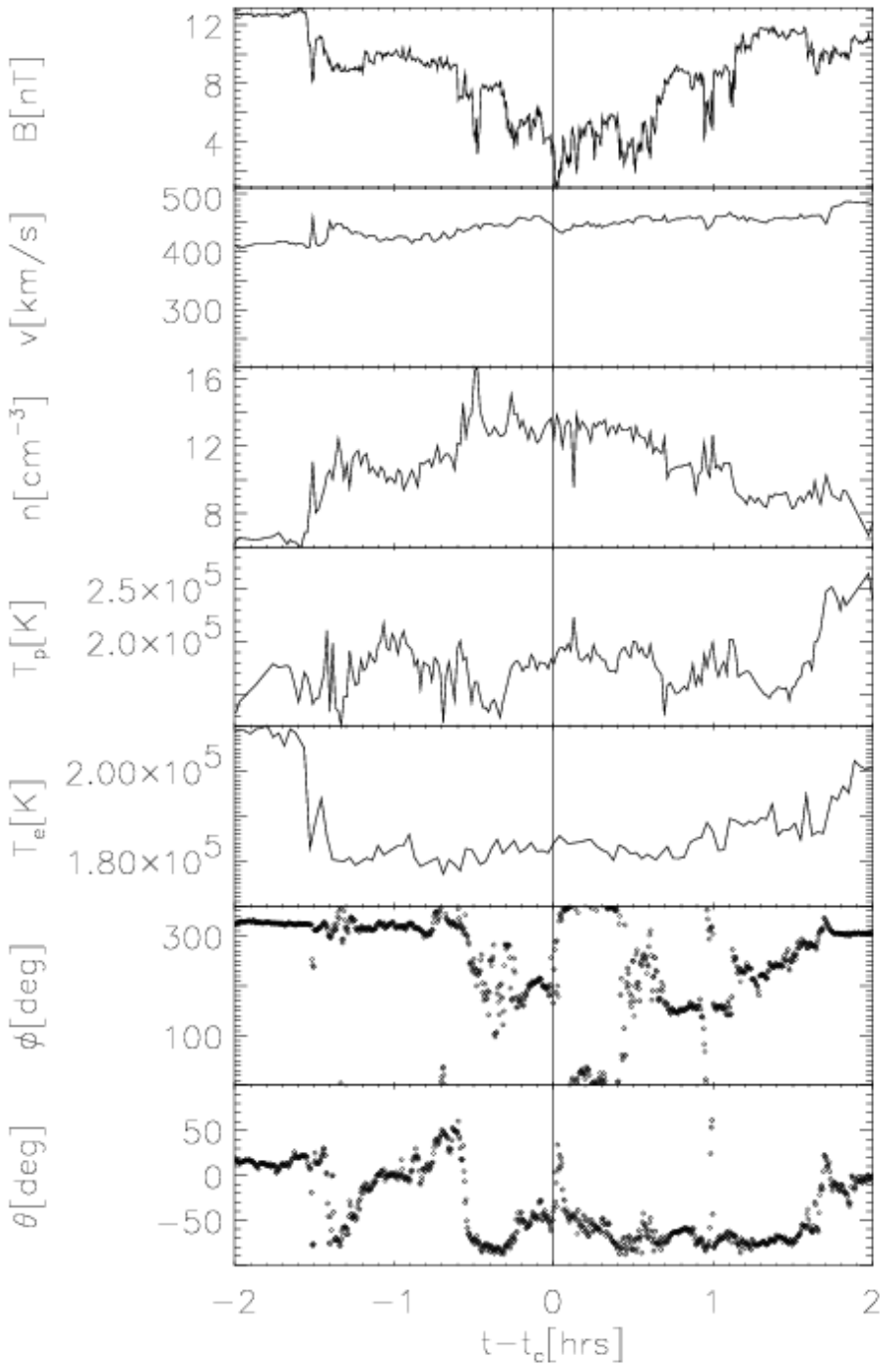

Figure 6. Plasma data from MAG and SWEPAM for the event during April 17. We use the same format as in Figure 2.

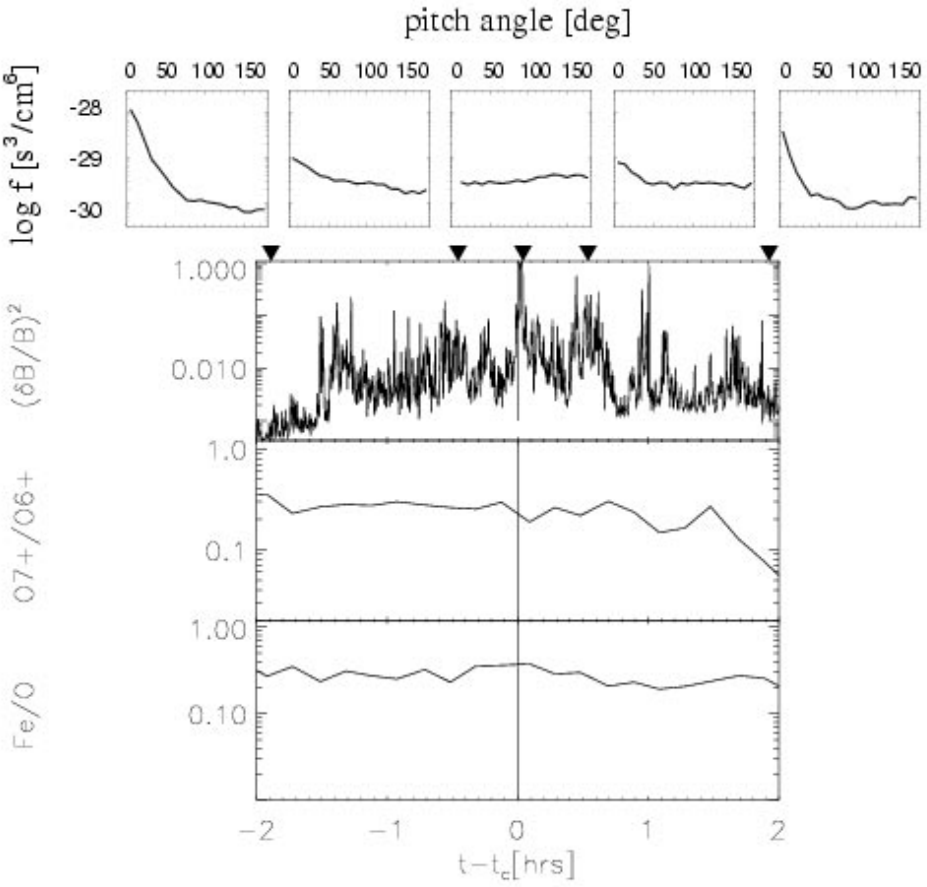

Figure 7. Electron pitch-angle and composition information for the event shown in Figure 6. The format is the same as in Figure 3.

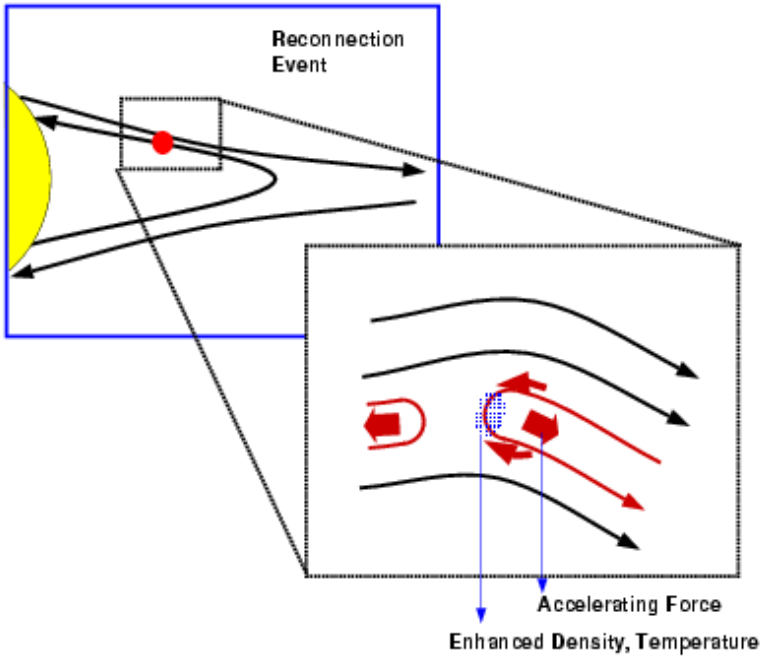

Figure 8. Sketch of the process resulting in the occurrence of extended magnetic depletions. For details, refer to text.

Table 1. Descriptions of the events used in this study. All events occurred in 1998.

Date	Time
February 9	4:00-6:00
March 10	11:45-12:45
April 3	4:00-5:30
April 9	4:00-6:00
April 13	20:00-1:00+1
April 16	7:00-8:30[a]
April 16	9:00-10:00[a]
April 17	5:45-10:00
June 18	22:00-23:30
July 16	0:30-1:00
July 16	2:30-3:30
July 23	0:10-3:00

[a]No data avaibale from SWICS.